Title

Interferon-β induction heterogeneity during KSHV infection is determined by interferon-β enhanceosome transcription factors other than IRF3

Authors

Machika Kaku[*, †] and Marta Maria Gaglia[†]

Footnote

[*]Program in Immunology, Tufts Graduate School of Biomedical Sciences, Boston, MA

[†]Department of Medical Microbiology and Immunology, Institute for Molecular Virology, and Carbone Cancer Center, University of Wisconsin - Madison, WI

ORCIDs: 0000-0002-9921-0678 (M.K.); 0000-0002-1791-0663 (M.M.G.)

Address correspondence and reprint requests to Dr. Marta Gaglia, University of Wisconsin-Madison, 1525 Linden Dr, Madison, WI 53706. E-mail address: marta.gaglia@wisc.edu. Phone number: (608)263-5551

This work was supported by National Institutes of Health Grant R01 CA268976 to M.M.G. and by the University of Wisconsin-Madison, Office of the Vice Chancellor for Research and Graduate Education with funding from the Wisconsin Alumni Research Foundation. The UWCCC Flow Cytometry Laboratory is supported by the UWCCC Cancer Center Grant P30 CA014520.

Abbreviations used in this article: A549, lung carcinoma cell line; ATF2, activating transcription factor 2; BC-3, KSHV-infected B cell line isolated from a patient with primary effusion lymphoma; BJAB, KSHV-negative B cell lymphoma line; casp-i, pan caspase inhibitor IDN-6556; c-Jun, Jun proto-oncogene; cGAS, cyclic GMP-AMP synthase; DAMP, damage associated molecular pattern; IRF3, interferon regulatory factor 3; ISG, interferon stimulated gene; KSHV, Kaposi's sarcoma-associated herpesvirus; NFKB1, nuclear factor kappa B subunit

1 or p50; PAMP, pathogen associated molecular pattern; PRR, pathogen recognition receptor; scRNA-seq, single cell RNA sequencing; STING, stimulator of interferon genes; RelA, RELA proto-oncogene or p65; TBK1, TANK-binding kinase 1; TPA, 12-O-tetradecanoylphorbol-13-acetate or PMA

Abstract

Strict regulation of type I interferons (IFN) is vital for balancing tissue damage and immunity against infections. We previously found that during Kaposi's sarcoma-associated herpesvirus infection, IFN induction was limited to a small percentage of infected B cells. This heterogeneity was not explained by viral gene expression. Here, we used a fluorescent reporter and fluorescence-activated cell sorting to investigate the source of this heterogeneity. Surprisingly, the canonical IFN induction pathway culminating in the activation of the IRF3 transcription factor was similar between cells that made high vs. low/no IFN-β. In contrast, the activation or expression of two other IFN transcription factors, NF-κB and AP-1, correlated with heterogeneous IFN-β induction. Our results suggest that at the level of individual cells, IRF3 is crucial as a pathogen detection signal, but NF-κB and AP-1 are limiting for IFN-β induction.

Introduction

Type I and III interferons such as interferon-β (IFN-β) and interferon-λ (IFN-λ) are potent cytokines that defend mammals against viral infections. As a key component of innate immunity, they orchestrate antiviral defense by signaling through the IFNAR1/2 and IFNLR1/IL10Rβ receptor complexes, respectively, and inducing hundreds of interferon-stimulated genes (ISGs) (1). ISGs encode proteins that modulate cell physiology to antagonize viral replication (2). However, IFNs are well known to be a double-edged sword because of their powerful effects on cell and tissue physiology. While insufficient IFN-related inflammation leaves the host susceptible to infections, excessive IFN-related inflammation causes tissue damage and contributes to autoimmune disease development (3-5). Therefore, IFN-β and other type I and III IFNs are carefully regulated, and multiple host regulatory mechanisms have evolved to ensure their expression only under appropriate conditions.

An emerging dimension of IFN regulation is transcriptional heterogeneity at the single-cell level. This aspect of interferon regulation has become clear in the growing number of single-cell RNA sequencing (scRNA-seq) analyses of infected cells. We and others have found only a small percentage (<10%) of virus-infected cells produce IFN-β or IFN-λ (6-18). This has been reported in infections with the RNA viruses Influenza A Virus (7, 10, 11, 14-17), Newcastle Disease Virus (18, 19), West Nile Virus (13), and SARS-CoV-2 (9), as well as the DNA viruses Herpes Simplex Virus 1 (12) and Human Cytomegalovirus (8), in addition to our results with Kaposi's sarcoma-associated herpesvirus (KSHV) (6). Since subversion of type I and III IFN is a key evolutionary tactic for viruses in the virus-host arms race, heterogeneity in the expression and activity of IFN-inhibiting viral proteins has been proposed as the reason for heterogeneous IFN expression (15, 20). However, we and others have found that viral gene expression heterogeneity does not fully account for the observed IFN heterogeneity during infection with KSHV, Influenza A Virus, Sendai Virus, and Newcastle Disease Virus (6, 11, 19, 21, 22), suggesting there are also cellular components to heterogeneous IFN induction. Limiting the percentage of cells producing type I and III IFN in an infected population may allow for optimal distribution of the cytokine and activation of surrounding cells without reaching a dangerous level. However, the mechanisms restricting IFN induction to a few cells remain elusive.

Type I and III IFNs are induced in response to pathogen-associated molecular patterns (PAMPs), such as nucleic acids with aberrant characteristics, or damage-associated molecular

patterns (DAMPs) due to infection-induced stress. PAMPs and DAMPs are recognized by pattern recognition receptors (PRRs), such as RIG-I-like receptors, Toll-like receptors, and cyclic GMP-AMP synthase (cGAS), which then activate signaling cascades that result in transcription of IFN-β. While different PRRs rely on different signaling adaptors, their signaling pathways generally converge on the kinase TANK-binding kinase 1 (TBK1), which phosphorylates the key transcription factor interferon regulatory factor 3 (IRF3). IRF3 is the best studied IFN-β transcription factor, but IFN-β transcription requires a complex of transcription factor complexes that make up the IFN-β enhanceosome (23). In addition to IRF3, the IFN-β enhanceosome includes the nuclear factor kappa-light-chain-enhancer of activated B-cells (NF-κB) and activator protein 1 (AP-1) complexes. The coordination of multiple transcription factors provides a secure barrier for the appropriate induction of IFN-β. However, how this restriction plays out at the single-cell level remains unknown.

Previous studies that have detected IFN-β induction heterogeneity have proposed different explanations. Some studies have suggested that the promoter firing step is inherently stochastic (19, 24). In contrast, Zhao et al. found that the fraction of IFN-β expressing cells remains constant through recloning and cell division, pointing to genetically programmed stochasticity, but were not able to narrow it down to specific factors (21). We previously found that KSHV hijacks the function of host caspases to prevent IFN-β induction when KSHV re-enters the replicative (lytic) cycle from a dormant (latent) infection state (25). Adding a small molecule caspase inhibitor restores activation of the cGAS PRR (6) and results in IFN-β induction (25). While the amount of IFN-β produced under these conditions based on ELISA measurements was substantial (25), subsequent experiments revealed that the IFN-β came from a small population of cells (6). scRNA-seq analysis revealed that IFN-β induction is highly heterogeneous, with less than 4% of infected cells responsible for producing significant amounts of IFN-β (6). The IFN-β heterogeneity was only partially explained by heterogeneous viral gene expression. We did not detect any IFN-β in cells that were latently infected or in the very late stages of lytic replication. We attribute this result to a lack of virus detection in the first case and potent inhibition in the second. However, 46% of the cells had a gene expression pattern corresponding to the early stages of the lytic cycle, but only 6% of them produced IFN-β. When we compared IFN-β positive and negative cells within this group, we did not find any viral gene that was specifically missing in IFN-β-producing cells, as would be expected for a

heterogeneously expressed viral IFN suppressor (25). These findings suggested to us that there is an additional, likely cellular, source of IFN-induction heterogeneity in this system.

In this study, we used the KSHV lytic infection and caspase inhibition system to probe further the source of heterogeneous IFN-β production during viral infection, as it provides robust and sustained induction of IFN. We developed a tool for separating cells expressing high vs. low levels of IFN-β and found that surprisingly, the canonical IFN induction pathway culminating in IRF3 activation was activated equally in both populations. However, activation or levels of other components of the IFN-β enhanceosome were heterogeneous and better correlated with IFN-β induction. Thus, we establish that in our system, activation of the NF-κB component RelA and baseline levels of the AP-1 component ATF2 are the limiting factors for IFN-β transcription at a single-cell level. This study highlights the nuanced mechanics behind the induction of a key component of our body's antiviral response, and for the first time identifies cellular factors whose heterogeneity contributes to limiting IFN-β induction to a small subpopulation of cells during infection.

Materials and Methods

Cell lines, reagents, and treatments

All cells were cultured at 37°C and 5% CO_2. HEK293T cells were grown in Dulbecco's modified Eagle's medium (DMEM; Life Technologies) supplemented with 10% fetal bovine serum (FBS; Hyclone). BC-3 cells and derivatives were maintained at a density of $0.5x10^6$ cells/mL in Roswell Park Memorial Institute medium (RPMI; Life Technologies) supplemented with 20% FBS, 2 mM GlutaMAX (Gibco), and 55 μM β-mercaptoethanol (BME; Gibco). BC-3-IFN-β-tdTomato cells were generated as described in Lent, Tabtieng, et al., 2022 (6). For reactivation, BC-3 cells were seeded at a density of $0.5x10^6$ cells/mL and treated with 20 ng/mL TPA (12-O-tetradecanoylphorbol-13-acetate; MilliporeSigma 5244001MG) dissolved in dimethylsulfoxide (DMSO; Sigma Aldrich Fine Chemicals Biosciences). Reactivation rates were checked for all experiments and are plotted in Supp. Fig. 1). Where indicated, cells were treated with vehicle (DMSO), 10 μM IDN-6556 (Emricasan; Selleck Chemical LLC S777525MG), and a mixture of neutralizing antibodies against type I IFNs at 1:500 dilution (PBS Assay Science 39000-1).

Fluorescence-activated cell sorting

100 mL of BC-3 cells were seeded at a density of $0.5x10^6$ cells/mL and treated with TPA, IDN-1665, and, where indicated, anti-IFN antibody mixture as described above. After two days, they were collected and sorted based on tdTomato fluorescence on BD FACSAria III at the UW Carbone Cancer Center Flow Cytometry Laboratory core facility. A DAPI stain (which only stains dead cells in the absence of permeabilization) was used to remove dead cells from the analysis. Gates for tdTomato fluorescence were drawn based on a negative control of BC-3 cells that lack the reporter system. BC-3 cells lacking the reporter system were treated identically as the sorted reporter cells. In each experiment, about $80x10^6$ cells were sorted. $3x10^6$ tdTomato+ and $12x10^6$ tdTomato- cells were collected. Sorted cells were pelleted and resuspended in 1 mL of PBS each. 100 μL of cell suspension were used for RNA extraction and 900 μL for protein extraction. Bulk controls were prepared in parallel with 4 mL of BC-3 cells seeded at a density of $0.5x10^6$ cells/mL and treated as indicated for 2 days. The bulk control cells were pelleted and

resuspended in 1 mL of PBS. 50 µL of cell suspension were used for RNA extraction, 450 µL for protein extraction, and 500 µL for flow cytometry to determine reactivation efficiency.

RT-qPCR

RNA samples were collected from BC-3 cells reactivated for 2 days as described above or treated with vehicle. For experiments not involving sorting, 4 mL of BC-3 cells were used and collected as described above for bulk control samples. In both cases, cells to be lysed were pelleted by centrifugation and resuspended in RNA lysis buffer (Zymo research). Total RNA was extracted using the Quick-RNA MiniPrep kit (Zymo research) following the manufacturer's protocol. cDNA was prepared using an iScript cDNA synthesis kit (Bio-Rad) following the manufacturer's protocol. Real-time quantitative PCR (RT-qPCR) was performed using iTaq Universal SYBR green Supermix (Bio-Rad) in a CFX Connect real-time PCR detection system (Bio-Rad). No-template and no-RT controls were included in each replicate. In all cases, 18S rRNA levels were used as an internal standard to calculate relative mRNA levels. CFX Manager software was used to analyze the data. Primers are listed in Table S1.

Protein analysis

Protein samples were collected from BC-3 cells reactivated for 2 days as described above or treated with vehicle. For samples not undergoing sorting, 4 mL of BC-3 cells were used and collected as described for bulk control samples. In both cases, cells to be lysed were pelleted by centrifugation and resuspended in an NP-40-only buffer (50 mM Tris-HCl pH 7.4, 150 mM NaCl, 1 mM EDTA, 0.5% NP-40) supplemented with a broad-spectrum protease inhibitor mixture (Thermo Scientific A32955) and a broad-spectrum phosphatase inhibitor mixture (Thermo Scientific A32957). Protein concentration was determined by Bradford method (Bio-Rad 5000006), and Laemmli buffer (Bio-Rad) was added to samples before being denatured at 95°C for 5 min. Samples were separated by SDS-PAGE and transferred to polyvinylidene difluoride membranes (PVDF; Fisher Scientific IPFL00010) using semi-dry Trans-Blot Turbo Transfer System (Bio-Rad). Membranes were blocked in 5% bovine serum albumin (BSA; Fisher BioReagents BP1600-100) in TBST. All antibodies used were diluted 1:1000 in 5% BSA in TBST for staining. The following Cell Signaling Technologies antibodies were used: IRF3 (D6I4C, no.11904), phospho-IRF3 Ser386 (E7J8G, no.37829), TBK1 (D1B4, no.3504),

phospho-TBK1 Ser172 (D52C2, no.5483), ATF2 (D4L2X, no.35031), c-Jun (60A8, no.9165), NF-κB p65/RelA (D14E12, no.8242), phospho-NF-κB p65/RelA Ser536 (93H1, no.3303). In addition, antibodies against β-actin (Abcam, ab8229) were used for loading controls. Secondary horseradish peroxidase (HRP)-conjugated antibodies (goat anti-rabbit and rabbit anti-goat IgG) were purchased from Southern Biotechnology (no.4030-05, no.OB6106-05) and used at 1:5000 in 5% BSA in TBST. All membranes were exposed using SuperSignal West Pico PLUS Chemiluminescent Substrate (Thermo Scientific) and imaged with an iBright FL1000 imaging system (Thermo Scientific).

Flow cytometry analysis

BC-3-IFN-β-tdTomato cells were fixed with 4% paraformaldehyde (PFA; Electron Microscopy Sciences) in phosphate buffer saline (PBS) for 15 min at room temperature and washed twice with PBS. Then, the cells were permeabilized by incubating in ice cold 90% methanol (diluted in 0.5% BSA in PBS) for 5 mins on ice and washed twice with 0.5% BSA in PBS. For measurements of interferon-β reporter activity, cells were then filtered through a 35 μm strainer (Chemglass Life Sciences CLS4380009) and analyzed. For assessment of reactivation efficiency, cells were then stained for a KSHV lytic infection marker, ORF45. They were incubated with antibodies against KSHV ORF45 (Thermo Fisher MA514769) at 1:100 dilution for 1 hr at room temperature, washed twice, and then stained with Alexa Fluor 647 (AF647)-conjugated secondary antibody at 1:500 dilution (Thermo Fisher A21236) for 30 min at room temperature in the dark. 0.5 % BSA in PBS was used for all incubations and washes. After two washes, cells were resuspended in 0.5% BSA in PBS and filtered as above for analysis. Cells were collected by centrifugation at 500 x *g* for 5 min between all washes/incubation. AF647 fluorescence and tdTomato fluorescence were quantified by flow cytometry on a Thermo Fisher Attune NxT V6 cytometer at the UWCCC Flow Cytometry Laboratory. AF647 fluorescence was gated based on the corresponding latently infected and vehicle (DMSO)-treated cells. tdTomato fluorescence was gated based on BC-3 cells that lack the reporter system. 300,000 events were collected per sample.

Single cell RNA sequencing analysis

A dataset obtained from KSHV-infected iSLK.219 cells previously published in Lent, Tabtieng, et al., 2022 (6) (GSE190558) was re-analyzed in the current study by extracting prepared Seurat matrices. FindMarkers function of Seurat was used to identify genes whose expression best correlated with IFNB1.

Statistics

All statistical analysis was performed using GraphPad Prism version 10.3.0 or later (GraphPad Software, Boston, MA USA; www.graphpad.com). Statistical significance was determined by One-way ANOVA followed by a *post hoc* multiple-comparison test (Dunnett) when multiple comparisons were required. All data are plotted as means and standard deviations. All plots represent mean +/- standard deviation.

Results

A fluorescent tdTomato reporter driven by a minimal human IFN-β promoter distinguishes cells that express high vs. low levels of IFN-β

Using scRNA-seq, we previously found that a very small fraction of KSHV-infected cells produce IFN-β when the virus is reactivated and caspases are inhibited (6). We calculated this fraction to be 3.8% of the total population and 6% of the infected cells in the early stage of the lytic cycle. Nonetheless, the rare IFN-β producing cells clustered together in our scRNA-seq data, suggesting that they have different characteristics from other cell populations. To identify factors involved in IFN-β regulation, we sought to separate and compare IFN-β producing and non-producing cells. We previously engineered a tdTomato reporter driven by two copies of a 303 bp minimal promoter sequence from the human *IFNB1* gene (Fig. 1A) and created stable cell lines with this reporter in BC-3 cells, KSHV-infected B cells isolated from a patient with primary effusion lymphoma (BC3-IFN-βp-tdTomato cells) (6). The design of the promoter was based on previous reporters that used two copies of the minimal IFN-β promoter sequence followed by luciferase or chloramphenicol acetyltransferase (26-28). tdTomato was selected because it is the brightest fluorescent protein whose signal is well separated from autofluorescence, which appears in the green channel (29-31). While our original scRNA-seq study was performed in KSHV-infected epithelial cells, the iSLK.219 system (6), we chose BC-3s for subsequent experiments because they are more biologically relevant, as B cells but not epithelial cells are the target of KSHV infection in patients. Moreover, the virus in iSLK.219 cells expresses GFP and RFP fluorescent reporters (32) that restrict our options for fluorescent markers. In BC-3 cells, the KSHV lytic cycle can be reactivated using the protein kinase C activator TPA (Supp. Fig. 1). As we previously reported (6), treating BC3-IFN-βp-tdTomato reporter cells with TPA and the pan-caspase inhibitor IDN-6556 induced IFN-β compared to no treatment, TPA alone, or the caspase inhibitor alone (Fig. 1B). Also as we previously reported (6), we found that only a small percentage of BC3-IFN-βp-tdTomato reporter cells expressed tdTomato (not shown). TPA-mediated reactivation is the most commonly used method of reliably reactivating KSHV in primary effusion lymphoma cell lines such as BC-3 cells (33). However, TPA can drive activation of multiple signaling pathways involved in growth, apoptosis, and differentiation through activation of protein kinase C (34, 35). Therefore, to ensure that the use of TPA would

not confound our studies, we measured IFN induction in an uninfected EBV- and KSHV-negative B cell lymphoma line, BJAB cells, treated with TPA and the pan-caspase inhibitor IDN-6556 (36, 37). We found that neither IFN-β nor IFN-λ1 were induced after TPA and IDN-6556 treatment in uninfected BJAB cells (Supp. Fig. 3). Therefore, we concluded that the IFN induction in BC-3 cells was indeed due to KSHV lytic reactivation and virus sensing, not just TPA addition, and that this system could be used for further experiments.

To isolate cells expressing high and low IFN-β levels, we subjected the lytically reactivated BC3-IFN-βp-tdTomato reporter cells treated with caspase inhibitors to fluorescence-activated cell sorting (FACS) and collected tdTomato+ and tdTomato- cells (Supp. Fig. 2). To confirm that this reporter results in separation of cells based on IFN-β status, we measured tdTomato and IFN-β RNA levels in the sorted samples. Importantly, we found that the endogenous IFN-β transcript was enriched in the tdTomato+ cells and depleted in the tdTomato- cells, as was tdTomato mRNA (Fig. 1C,D). This result demonstrates that FACS of the BC3-IFN-βp-tdTomato reporter line allows us to separate cells producing high and low levels of IFN-β within a population.

IFN-β is not stochastically induced

Some groups have proposed that heterogeneous expression of IFN-β may be generated by stochasticity of IFN-β promoter firing (19, 24). This model posits that the signals and activated proteins needed for IFN-β induction are present in all infected cells, but transcription of IFN-β only occurs stochastically in some cells. To test this hypothesis, we took advantage of the fact that pathogen sensing often induces type III IFNs like IFN-λ1 in addition to type I IFNs and that the signaling cascade and transcription factors that regulate type I and III IFNs are very similar (38). However, since IFN-β and IFN-λ1 have separate promoters and are located on different chromosomes, they should not be expressed by the same cells if their transcription upon pathway activation is stochastic. Contrary to the stochasticity model, our results indicated that IFN-β and IFN-λ1 were induced in the same rare cells. We previously reported that based on the scRNA-seq data, IFN-λ1 was also induced in iSLK.219 cells upon lytic reactivation and caspase inhibitor treatment at similar levels to IFN-β (6). We have since performed further analysis of the scRNA-seq data and found that the IFN-λ1 transcript had the closest correlation to the IFN-β transcript. 31% of IFN-β-expressing cells also expressed IFN-λ1, compared to only 8% of IFN-β-negative

cells (data not shown). We also analyzed IFN-λ1 expression after sorting BC3-IFN-βp-tdTomato cells. Like IFN-β, IFN-λ1 was induced in BC-3 lytic cells treated with caspase inhibitors (Fig. 2A). Moreover, IFN-λ1 was enriched and depleted in concert with IFN-β in the tdTomato-positive and negative cells, respectively, indicating that it was likely expressed in the same cells (Fig. 2B). Therefore, we conclude that IFN-β and IFN-λ1 are not stochastically transcribed but coordinately regulated. Moreover, the fact that they are expressed in the same rare subset of KSHV-infected cells suggests that the same upstream determinant leads to heterogeneous type I and III IFN induction.

TBK1 and IRF3 activity does not explain IFN-β heterogeneity

The results above suggested that activation of the IFN-β induction pathway rather than IFN-β transcription is heterogeneous. However, there are several signaling steps in this pathway that could be the bottleneck in determining whether cells transcribe IFN-β. Therefore, we monitored the activation of the IFN-β induction pathway, particularly the later steps of kinase and transcription factor activation. We previously found that in our system, IFN-β induction is driven by the DNA sensing cGAS-STING pathway (6) and requires activation of the kinase TBK1 (25). We thus tested whether TBK1 was activated only in the cells that induce IFN-β by comparing levels of phosphorylated TBK1 in lytically reactivated, caspase inhibitor-treated cells sorted based on tdTomato status. We used poly(I:C)-treated A549 cells as positive controls for activation of the pathway. In every experiment, we confirmed that tdTomato-based sorting resulted in the expected enrichment and depletion of IFN-β mRNA in tdTomato+ and tdTomato- cells, respectively (RNA measurements are shown in Fig. 1C). Surprisingly, we observed no difference in activated (phosphorylated) TBK1 between IFN-β high and low cells (Fig. 3). Since TBK1 phosphorylates and activates the well-characterized IFN-β transcription factor IRF3, we also tested whether IRF3 was differentially activated in the IFN-β high vs. low cells. Like TBK1, we observed no difference in IRF3 phosphorylation between the two populations (Fig. 3). Therefore, while both TBK1 and IRF3 were active in lytic cells treated with caspase inhibitors, as expected, their activation alone was not predictive of IFN-β induction (Fig. 3). This result indicates that the canonical IFN induction pathway is activated in many, likely most, infected cells, but that regulation by an important factor besides IRF3 keeps IFN-β induction limited to a small fraction of the population.

AP-1 and NF-κB are the determinants of IFN-β heterogeneity

IRF3 activation is often assumed to lead to IFN-β transcription and phosphorylation of IRF3 is commonly used as a proxy for IFN induction. However, the IFN-β enhanceosome contains two additional transcription factor complexes: AP-1, formed by c-Jun and ATF2, and NF-κB, formed by the RelA/p65 and NFKB1/p50 subunits (39-41). While the AP-1 and NF-κB complexes in other settings can include other members of the c-Jun, ATF2, and NF-κB families, the specific proteins listed above are required for IFN-β transcription during viral infections (41). Moreover, at least NF-κB and IRF3 are also transcription factors for IFN-λ1 (42). However, the exact pathways activating AP-1 and NF-κB in the IFN-β induction pathway and their relation to activation of cGAS and other PRRs are not well understood. Given that IRF3 activation did not explain IFN-β heterogeneity, we considered the possibility that AP-1 and/or NF-κB might be the determinants of heterogeneous IFN-β induction in our system. We previously reported that the expression of NF-κB family members was enriched in IFN-β-expressing cells based on scRNA-seq analysis of KSHV-infected iSLK.219 cells treated with caspase inhibitors (6). We reanalyzed the scRNA-seq dataset and found that this was also the case for the AP-1 components (not shown). To further explore the relationship between IFN-β and these transcription factors, we focused on the IFN-β producing cells by separating the IFN-β expressing clusters (clusters 9 and 11) into IFN-β-positive and negative cells (Fig. 4A). Both the NF-κB components RelA and NFKB1/p50 and the AP-1 component c-Jun were enriched in the IFN-β-positive cells (Fig. 4A). This enrichment was particularly evident when anti-interferon blocking antibodies were added to prevent paracrine and autocrine signaling from IFN-β, because most of these genes were induced by IFN-β signaling (Fig. 4B). To note, we also observed an enrichment of IRF3 RNA in the IFN-β-producing cells in the scRNA-seq data, even though we did not detect enrichment at the protein level in BC-3 cells (Fig. 3B). We then tested whether NF-κB and AP-1 were enriched at the protein level in BC-3 cells expressing high levels of IFN-β. To reduce confounds from paracrine signaling, we repeated the sorting experiments with anti-IFN blocking antibodies. The antibody treatment effectively blocked responses to IFN, as shown by a reduction in the levels of the IFN-stimulated gene MxA (Supp. Fig. 1C). We still observed IFN-β induction in the lytic cells treated with caspase inhibitors after antibody treatment, although it was decreased (Fig. 4C), which was consistent with our results in iSLK.219 cells (6). It is likely that the anti-IFN

blocking antibodies prevent a positive feedback mechanism that enhances IFN-β induction (43). Importantly, we still observed enrichment of IFN-β RNA in the sorted tdTomato+ reporter cells, and similar levels of total and phosphorylated IRF3 in both tdTomato+ and tdTomato- cells (Fig. 4D,E). In contrast, we observed an enrichment in the AP-1 component ATF2 in tdTomato+ vs. tdTomato- cells, indicating that ATF2 levels are higher in cells that express high levels of IFN-β (Fig. 4F). Interestingly, total ATF2 levels did not change between conditions in unsorted (bulk) samples, indicating that ATF2 expression was not induced during infection and/or by caspase inhibitor treatment. Instead, these results suggest that basal expression of ATF2 is variable and that IFN-producing cells had higher ATF2 levels prior to lytic reactivation (Fig. 4F). Levels of the other AP-1 component c-Jun were variable across replicates, but in two out of three replicates a unique shorter isoform was detected in the sorted IFN-β high cells (Fig. 4F). However, this shorter c-Jun isoform was also induced by treatment of uninfected BJAB cells treated with TPA and caspase inhibitors (Supp. Fig. 3C), suggesting that its appearance may be unrelated to viral replication and IFN induction, as IFN-β is not induced in uninfected cells (Supp. Fig. 3A). In addition, sorting for IFN-β high cells enriched for cells containing phosphorylated RelA, one of the NF-κB components, whereas there was little to no phosphorylated RelA in the IFN-β low cells. This result points to RelA activation only in IFN-β high cells (Fig. 4G). Overall, these results point to a role for ATF2 and phospho-RelA in cell-specific IFN-β induction. Moreover, our results indicate that elevated ATF2 levels are likely a predictor of IFN-β induction, while RelA is likely activated in response to a stimulus but may serve to potentiate IFN transcription (Fig. 5).

Discussion

In this study, we reveal that the IFN-β enhanceosome components AP-1 and NF-κB, but not IRF3, determine whether individual cells induce IFN-β during KSHV and caspase inhibition. We found that protein levels of the AP-1 factor ATF2 and phosphorylation of the NF-κB factor RelA are higher in cells that express high levels of IFN-β than in cells that express minimal IFN-β. In particular, ATF2 levels are not upregulated under IFN-inducing conditions based on bulk analysis, but our results indicate that sorting for cells with high IFN-β enriched for cells with high ATF2. The implication of this finding is that ATF2 heterogeneity precedes viral reactivation and only cells with higher ATF2 are able to respond to pathogen cues by turning on IFN-β. In contrast, RelA is only activated under IFN-inducing conditions, which suggests a possible bottleneck to its activation in most cells. Our findings thus support a model in which IFN-β inducibility during KSHV lytic replication is limited to a rare fraction of cells with baseline elevated ATF2 levels, and the ability to activate NF-κB. While IRF3, AP-1, and NF-κB have long been known to regulate IFN transcription, their heterogeneity at the single-cell level had not previously been reported. Moreover, this is the first description of the unique role of AP-1 and NF-κB in controlling which individual cells make IFN.

Host regulation of IFN-β is important given its potent effects on both the host and pathogen through autocrine and paracrine induction of hundreds of ISGs. Insufficient induction of ISGs can lead to susceptibility to infection, while excessive IFN-related inflammation can lead to autoimmune disorders and excessive tissue damage. A system in which the barrier for IFN-β induction is very high may provide an appropriate level of innate immune alarm by limiting IFN-β expression to a small fraction of infected cells. The fact that many viral infections display heterogeneous IFN induction in a way that is not fully explained by viral factors (11, 19, 21, 22), in combination with our results, suggests that an important part of the mechanism of IFN regulation is rooted in cellular heterogeneity. Furthermore, heterogeneous expression of other cytokines such as IL-2 (44), IL-4 (45, 46), IL-5 (47), and IL-10 (48) has been reported, suggesting this is an important mode of immune regulation.

Interestingly, while IRF3 and TBK1 are required for IFN induction following PAMP/DAMP signaling, here we found they are not sufficient. Although IRF3 activation is often used as a proxy for IFN-β induction, especially in studies of viral infections, our results indicate that this one-to-one relationship is not true at the level of individual cells. Indeed, both

TBK1 and IRF3 appear to be activated regardless of the IFN status of the cells. Most likely, the upstream components of the IFN induction pathway, including the PRR (cGAS in this case), are also activated regardless of the IFN status of the cells. Instead, our results point to the other IFN-β enhanceosome factors, AP-1 and NF-κB, as the limiting factors that determine IFN-β induction in individual cells. We propose a model where IRF3 serves as an indicator for infection, while AP-1 and NF-κB heterogeneity function to limit IFN-β induction to a small subset of cells among an infected population.

The regulation of AP-1 and NF-κB during IFN responses is not as well characterized as the activation of IRF3, although NF-κB is likely also activated downstream of STING (49). For AP-1, our results suggest that differences may precede infection, because at the bulk level there is no clear change in ATF2 levels. Therefore, the simplest interpretation for our results (Fig. 5) is that some cells have higher ATF2, and these cells are more abundant in the IFN-producing pool. In contrast, NF-κB is likely activated in a subset of cells under IFN-inducing conditions. While IRF3 and NF-κB may both be activated by STING (49), the fact that NF-κB is only phosphorylated in IFN-β high cells while IRF3 is phosphorylated equally in IFN-β high and low cells indicates that there must be a heterogenous bottleneck downstream of STING specifically for NF-κB activation.

While this study has shed light on the expression mechanics of IFN-β during KSHV infection, the mechanism of IFN heterogeneity may differ in other viral infections and cell types. Although IFN heterogeneity is a widespread feature of viral infection, reported by every study we have encountered, the PRRs and signaling pathways that lead to IFN induction vary (6-18, 50). Moreover, IFN-β expression patterns appear to differ between cell types. For example, a larger proportion of infected dendritic cells expresses IFN-β (19, 51, 52) compared to other cell types, such as fibroblasts and epithelial cells (6-16). Flexibility in tailoring the IFN response to factors such as cell type, viral load, and PAMP type is likely evolutionarily beneficial in mounting an appropriate immune response. More studies identifying the determinants of IFN expression are needed to parse out the ubiquity vs. uniqueness of our findings.

Although our findings indicate that there is a high barrier to IFN-β induction, results from studies using Sendai virus suggest that heterogeneity of IFN-β induction is not due to a complete inability of some cells to induce IFN-β. Infection with a highly inflammatory strain of Sendai virus (the Cantell strain) induced IFN-β expression in 99% of infected A549 cells (11, 52). In

comparison, only 0.48% of A549 cells expressed IFN-β during infection with influenza A virus (11). This indicates that IFN-β regulation can be overridden given excessive stimuli such as the defective-interfering viral genomes that characterize the Sendai virus strain Cantell (53). These observations also suggest that the strength or abundance of the stimulus may matter. Indeed, strong IFN inducers like Newcastle Disease Virus, Sendai virus strain Cantell, or the potent PAMP mimetic poly(I:C) induce IFN-β in a larger proportion of cells (10-99%) (21, 22, 50, 51, 54-57) compared to other viral infections and treatments (1-10%) (6-17). Unfortunately, we have been unable to test whether the relationship between the strength of the stimulus and the percentage of IFN-expressing cells is also true in KSHV-infected BC-3 cells, as we have not identified a stronger stimulus that worked in this line. In order to isolate the cells that express IFN-β, the cells need to be active and viable for long enough for the tdTomato fluorescent protein to express and accumulate to detectable levels. Commonly used IFN-inducing stimuli (poly(I:C), 2'3'-cGAMP, STING agonist diABZI, TLR7 agonist imiquimod, and plasmid DNA) either did not induce IFN-β expression in BC-3 cells or induced cell death before we could assess tdTomato production (data not shown). IFN-β induction through KSHV reactivation and caspase inhibition allows for sustained IFN-β induction without inducing cell death, which gives us a unique tool to study the elusive phenomena of cellular heterogeneity and IFN-β induction.

There are some limitations to our study. First, the minimal IFN-β promoter used in our reporter lacks the native chromatin environment and potential long-range promoter elements. Our reporter system also did not fully recapitulate IFN-β kinetics, as only cells that had sustained IFN-β promoter activity were detectable during FACS. However, despite these imperfections, we were able to successfully separate the rare cells that expressed high levels of IFN-β (Fig. 1C). Also, while our results point to cellular heterogeneity as a major determinant of IFN-β regulation, we cannot completely rule out the possibility that the heterogeneity of AP-1 and NF-κB is regulated by the virus. While our scRNA-seq data did not reveal any correlation between viral genes and IFN-β expression (6), this method does not capture mutations that may have risen in individual cells. Moreover, the sequencing method was 3' end-directed, and many mRNAs in KSHV share 3' end sequences, preventing accurate measurement of some viral genes. We have also not repeated the scRNA-seq in the BC-3 cells. That said, to date there has been no report of a KSHV factor that blocks NF-κB activation in response to PRR activation or that regulates AP-1 levels, so there is no obvious viral explanation for the heterogeneity we observe. Lastly, while

TPA is a very effective inducer of lytic KSHV reactivation and is commonly used in KSHV research (33), it is also a known inducer of NF-κB in other setting. This is a potentially confounding variable. Our concern about this is reduced by the fact that treatments that induced IFN-β in infected BC-3 cells did not induce IFN-β or RelA phosphorylation in the uninfected BJAB cells, indicating that viral infection and not TPA treatment induces IFN-β. Moreover, our results are consistent between the BC-3 and iSLK.219 KSHV-infected cell lines, even though iSLK.219 cells are not treated with TPA to induce the lytic cycle. This also suggests that our results are not simply due to TPA treatment.

Despite the described limitations, this study points us to a new model of heterogeneous type I IFN transcription during viral infection as the result of inherent cellular heterogeneity in protein levels and protein activation. It is the first report of a role for cellular transcription factors in IFN induction heterogeneity. More studies are needed to pinpoint the earliest source of the heterogeneity and to examine the mechanism of enrichment and activation of AP-1 and NF-κB in the context of antiviral responses.

Acknowledgements

We thank members of the Gaglia laboratory for suggestions and feedback on the project and the manuscript. We thank the University of Wisconsin Carbone Cancer Center (UWCCC) Flow Cytometry Laboratory staff for technical and conceptual assistance.

References

1. Schoggins, J. W., S. J. Wilson, M. Panis, M. Y. Murphy, C. T. Jones, P. Bieniasz, and C. M. Rice. 2011. A diverse array of gene products are effectors of the type I interferon antiviral response. *Nature* 472.
2. Schoggins, J. W., and C. M. Rice. 2011. Interferon-stimulated genes and their antiviral effector functions. *Curr Opin Virol* 1: 7.
3. Taft, J., and D. Bogunovic. 2018. The Goldilocks Zone of Type I IFNs: Lessons from Human Genetics. *J Immunol* 201: 7.
4. González-Navajas, J. M., J. Lee, M. David, and E. Raz. 2012. Immunomodulatory functions of type I interferons. *Nat Rev Immunol* 12: 11.
5. Kobayashi, K. S., and R. A. Flavell. 2004. Shielding the double-edged sword: negative regulation of the innate immune system. *J Leukoc Biol* 75: 6.
6. Tabtieng, T., R. C. Lent, M. Kaku, A. Monago Sanchez, and M. M. Gaglia. 2022. Caspase-Mediated Regulation and Cellular Heterogeneity of the cGAS/STING Pathway in Kaposi's Sarcoma-Associated Herpesvirus Infection. *mBio* e0244622.
7. Hamele, C. E., A. B. Russell, and N. S. Heaton. 2022. In Vivo Profiling of Individual Multiciliated Cells during Acute Influenza A Virus Infection. *J Virol* 96.
8. Hein, M. Y., and J. S. Weissman. 2022. Functional single-cell genomics of human cytomegalovirus infection. *Nat Biotechnol* 40: 11.
9. Fiege, J. K., J. M. Thiede, H. A. Nanda, W. E. Matchett, P. J. Moore, N. R. Montanari, B. K. Thielen, J. Daniel, E. Stanley, R. C. Hunter, V. D. Menachery, S. S. Shen, T. D. Bold, and R. A. Langlois. 2021. Single cell resolution of SARS-CoV-2 tropism, antiviral responses, and susceptibility to therapies in primary human airway epithelium. *PLoS Pathog* 17.
10. Sun, J., J. C. Vera, J. Drnevich, Y. T. Lin, R. Ke, and C. B. Brooke. 2020. Single cell heterogeneity in influenza A virus gene expression shapes the innate antiviral response to infection. *PLoS Pathog* 16.
11. Russell, A. B., E. Elshina, J. R. Kowalsky, A. J. W. Te Velthius, and J. D. Bloom. 2019. Single-Cell Virus Sequencing of Influenza Infections That Trigger Innate Immunity. *J Virol* 93.

12. Drayman, N., P. Patel, L. Vistain, and S. Tay. 2019. HSV-1 single-cell analysis reveals the activation of anti-viral and developmental programs in distinct sub-populations. *Elife* 8.

13. O'Neal, J. T., A. Upadhyay, A. Wolabaugh, N. B. Patel, S. E. Bosinger, and M. S. Suthar. 2019. West Nile Virus-Inclusive Single-Cell RNA Sequencing Reveals Heterogeneity in the Type I Interferon Response within Single Cells. *J Virol* 93.

14. Russell, A. B., C. Trapnell, and J. D. Bloom. 2018. Extreme heterogeneity of influenza virus infection in single cells. *Elife* 7.

15. Killip, M. J., R. Jackson, M. Pérez-Cidoncha, E. Fodor, and R. E. Randall. 2017. Single-cell studies of IFN-β promoter activation by wild-type and NS1-defective influenza A viruses. *J Gen Virol* 98: 7.

16. Pérez-Cidoncha, M., M. J. Killip, J. C. Oliveros, V. J. Asensio, Y. Fernández, J. A. Bengoechea, R. E. Randall, and J. Ortín. 2014. An unbiased genetic screen reveals the polygenic nature of the influenza virus anti-interferon response. *J Virol* 88: 15.

17. Kallfass, C., S. Lienenklaus, S. Weiss, and P. Staeheli. 2013. Visualizing the beta interferon response in mice during infection with influenza A viruses expressing or lacking nonstructural protein 1. *J Virol* 87: 6.

18. Hu, J., G. Nudelman, Y. Shimoni, M. Kumar, Y. Ding, C. López, F. Hayot, J. G. Wetmur, and S. Sealfon. 2011. Role of cell-to-cell variability in activating a positive feedback antiviral response in human dendritic cells. *PLoS One* 6.

19. Hu, J., S. Sealfon, F. Hayot, C. Jayaprakash, M. Kumar, A. C. Pendleton, A. Ganee, A. Fernandez-Sesma, T. M. Moran, and J. G. Wetmur. 2007. Chromosome-specific and noisy IFNB1 transcription in individual virus-infected human primary dendritic cells. *Nucleic Acids Res* 35: 10.

20. Chen, S., J. A. L. Short, D. F. Young, M. J. Killip, M. Schneider, S. Goodbourn, and R. E. Randall. 2010. Heterocellular induction of interferon by negative-sense RNA viruses. *Virology* 407.

21. Zhao, M., J. Zhang, H. Phatnani, S. Scheu, and T. Maniatis. 2012. Stochastic expression of the interferon-β gene. *PLoS Biol* 10.

22. Rand, U., M. Rinas, J. Schwerk, G. Nöhren, M. Linnes, A. Kröger, M. Flossdorf, K. Kály-Kullai, H. Hauser, T. Höfer, and M. Köster. 2012. Multi-layered stochasticity and paracrine signal propagation shape the type-I interferon response. *Mol Syst Biol* 8.

23. Panne, D., T. Maniatis, and S. C. Harrison. 2007. An atomic model of the interferon-beta enhanceosome. *Cell* 129: 13.

24. Apostolou, E., and D. Thanos. 2008. Virus Infection Induces NF-kappaB-dependent interchromosomal associations mediating monoallelic IFN-beta gene expression. *Cell* 134: 7.

25. Tabtieng, T., A. Degterev, and M. M. Gaglia. 2018. Caspase-Dependent Suppression of Type I Interferon Signaling Promotes Kaposi's Sarcoma-Associated Herpesvirus Lytic Replication. *J Virol* 92.

26. Li, K., Z. Chen, N. Kato, K. Gale, and S. M. Lemon. 2005. Distinct poly(I-C) and virus-activated signaling pathways leading to interferon-beta production in hepatocytes. *J Biol Chem* 280: 9.

27. Guo, F., J. Mead, N. Aliya, L. Wang, A. Cuconati, L. Wei, K. Li, T. M. Block, J. T. Guo, and J. Chang. 2012. RO 90-7501 enhances TLR3 and RLR agonist induced antiviral response. *PLoS One* 7.

28. Gentili, M., J. Kowal, M. Tkach, T. Satoh, X. Lahaye, C. Conrad, M. Boyron, B. Lombard, S. Durand, G. Kroemer, D. Loew, M. Dalod, C. Thery, and N. Manel. 2015. Transmission of innate immune signaling by packaging of cGAMP in viral particles. *Science* 349.

29. Day, R. N., and M. W. Davidson. 2009. The fluorescent protein palette: tools for cellular imaging. *Chem Soc Rev* 38: 34.

30. Muzumdar, M. D., B. Tasic, K. Miyamichi, L. Li, and L. Luo. 2007. A global double-fluorescent Cre reporter mouse. *Genesis* 45: 13.

31. Surre, J., C. Saint-Ruf, V. Collin, S. Orenga, M. Ramjeet, and I. Matic. 2018. Strong increase in the autofluorescence of cells signals struggle for survival. *Sci Rep* 8.

32. Brulois, K. F., H. Chang, A. S. Y. Lee, A. Ensser, L. Y. Wong, Z. Toth, S. H. Lee, H. R. Lee, J. Myoung, D. Ganem, T. K. Oh, J. F. Kim, S. J. Gao, and J. U. Jung. 2012. Construction and Manipulation of a New Kaposi's Sarcoma-Associated Herpesvirus Bacterial Artificial Chromosome Clone. *J Virol* 86.

572 33. Cohen, A., C. Brodie, and R. Sarid. 2006. An essential role of ERK signalling in TPA-
573 induced reactivation of Kaposi's sarcoma-associated herpesvirus. *J Gen Virol* 87: 8.
574 34. Kikkawa, U., H. Matsuzaki, and T. Yamamoto. 2002. Protein kinase C delta (PKC delta):
575 activation mechanisms and functions. *J Biochem* 132: 9.
576 35. Duquesnes, N., F. Lezoualc'h, and B. Crozatier. 2011. PKC-delta and PKC-epsilon: foes
577 of the same family or strangers? *J Mol Cell Cardiol* 51: 9.
578 36. Menezes, J., W. Leibold, G. Klein, and G. Clemens. 1975. Establishment and
579 characterization of an Epstein-Barr virus (EBC)-negative lymphoblastoid B cell line
580 (BJA-B) from an exceptional, EBV-genome-negative African Burkitt's lymphoma.
581 *Biomedicine* 22: 9.
582 37. Arvanitakis, L., E. A. Mesri, R. G. Nador, J. W. Said, A. S. Asch, D. M. Knowles, and E.
583 Cesarman. 1996. Establishment and characterization of a primary effusion (body cavity-
584 based) lymphoma cell line (BC-3) harboring kaposi's sarcoma-associated herpesvirus
585 (KSHV/HHV-8) in the absence of Epstein-Barr virus. *Blood* 88.
586 38. Onoguchi, K., M. Yoneyama, A. Takemura, S. Akira, T. Taniguchi, H. Namiki, and T.
587 Fujita. 2007. Viral infections activate types I and III interferon genes through a common
588 mechanism. *J Biol Chem* 282: 6.
589 39. Lenardo, M. J., C. M. Fan, T. Maniatis, and D. Baltimore. 1989. The involvement of NF-
590 kappa B in beta-interferon gene regulation reveals its role as widely inducible mediator of
591 signal transduction. *Cell* 57: 8.
592 40. Wathelet, M. G., C. H. Lin, B. S. Parekh, L. V. Ronco, P. M. Howley, and T. Maniatis.
593 1998. Virus infection induces the assembly of coordinately activated transcription factors
594 on the IFN-beta enhancer in vivo. *Mol Cell* 1: 11.
595 41. Maniatis, T., J. V. Falvo, T. H. Kim, T. K. Kim, C. H. Lin, B. S. Parekh, and M. G.
596 Wathelet. 1998. Structure and function of the interferon-beta enhanceosome. *Cold Spring*
597 *Harb Symp Quant Biol* 63: 12.
598 42. Iversen, M. B., and S. R. Paludan. 2010. Mechanisms of type III interferon expression. *J*
599 *Interferon Cytokine Res* 30: 6.
600 43. Ma, F., B. Li, S. Liu, S. S. Iyer, Y. Yu, A. Wu, and G. Cheng. 2015. Positive feedback
601 regulation of type I IFN production by the IFN-inducible DNA sensor cGAS. *194* 4: 10.

44. Holländer, G. A. 1999. On the stochastic regulation of interleukin-2 transcription. *Semin Immunol* 11: 11.

45. Guo, L., J. Hu-Li, and W. E. Paul. 2004. Probabilistic regulation of IL-4 production in Th2 cells: accessibility at the Il4 locus. *Immunity* 20: 11.

46. Guo, L., J. Hu-Li, and W. E. Paul. 2005. Probabilistic regulation of IL-4 production. *J Clin Immunol* 25: 9.

47. Kelly, B. L., and R. M. Locksley. 2000. Coordinate regulation of the IL-4, IL-13, and IL-5 cytokine cluster in Th2 clones revealed by allelic expression patterns. *J Immunol* 165: 5.

48. Calado, D. P., T. Paixão, D. Holmberg, and M. Haury. 2006. Stochastic monoallelic expression of IL-10 in T cells. *J Immunol* 177: 7.

49. Ishikawa, H., and G. N. Barber. 2008. STING is an endoplasmic reticulum adaptor that facilitates innate immune signalling. *Nature* 455: 5.

50. Parekh, N., D. Winship, E. V. Dis, and D. B. Stetson. 2024. Regulation and Dynamics of IFN-β Expression Revealed with a Knockin Reporter Mouse. *J Immunol* 213: 11.

51. Shalek, A. K., R. Satija, J. Shuga, J. J. Trombetta, D. Gennert, D. Lu, P. Chen, R. S. Gertner, J. T. Gaublomme, N. Yosef, S. Schwartz, B. Fowler, S. Weaver, J. Wang, X. Wang, R. Ding, R. Raychowdhury, N. Friedman, N. Hacohen, H. Park, A. P. May, and A. Regev. 2014. Single-cell RNA-seq reveals dynamic paracrine control of cellular variation. *Nature* 510: 7.

52. Strahle, L., D. Garcin, and D. Kolakofsky. 2006. Sendai virus defective-interfering genomes and the activation of interferon-beta. *Virology* 351: 11.

53. Johnston, M. D. 1981. The characteristics required for a Sendai virus preparation to induce high levels of interferon in human lymphoblastoid cells. *J Gen Virol* 56: 10.

54. Patil, S., M. Fribourg, Y. Ge, M. Batish, S. Tyagi, F. Hayot, and S. Sealfon. 2015. Single-cell analysis shows that paracrine signaling by first responder cells shapes the interferon-β response to viral infection. *Sci Signal* 8.

55. Hwang, S. Y., K. Y. Hur, J. R. Kim, K. H. Cho, S. H. Kim, and J. Y. Yoo. 2013. Biphasic RLR-IFN-β response controls the balance between antiviral immunity and cell damage. *J Immunol* 190: 9.

632 56. Zawatzky, R., E. D. Maeyer, and J. D. Maeyer-Guignard. 1985. Identification of
633 individual interferon-producing cells by in situ hybridization. *PNAS* 82: 5.
634 57. Enoch, T., K. Zinn, and T. Maniatis. 1986. Activation of the human beta-interferon gene
635 requires an interferon-inducible factor. *Mol Cell Biol* 6: 10.
636

Figure legends

Figure 1. An IFN-β-promoter driven fluorescent reporter allows isolation of cells expressing high and low levels of IFN-β. A. Diagram of the IFN-βp-tdTomato reporter. Two copies of the 303 bp minimal promoter sequence for the human IFNB1 gene were cloned in front of the tdTomato fluorophore. This cassette was then introduced in BC-3 cells via lentiviral transduction leading to stable integration. **B-D.** BC3-IFN-βp-tdTomato reporter cells were treated with 20 ng/mL TPA for 48 hours to induce the lytic cycle ("lytic (TPA)") Where indicated, the cells were also treated with the pan-caspase inhibitor IDN-6556 at 10 μM ("casp-i"). IFN-β and tdTomato mRNA levels were measured by RT-qPCR and normalized to 18S rRNA. For **B**, IFN-β mRNA levels are plotted normalized to the lytic+casp-i sample. For **C and D** the lytic+casp-i treated samples were sorted based on tdTomato expression and the fold enrichment in IFN-β and tdTomato RNA levels compared to unsorted ("bulk") samples is plotted in $\log_{10}$ scale. n=6.

Figure 2. IFN-λ1 is expressed in the same set of cells that produce high levels of IFN-β, pointing to heterogeneity in the induction pathway rather than -stochastic IFN-β promoter firing. A. BC3-IFN-βp-tdTomato reporter cells were treated with 20 ng/ml TPA for 48 hours to induce the lytic cycle ("lytic (TPA)"). Where indicated, the cells were also treated with the pan-caspase inhibitor IDN-6556 at 10 μM ("casp-i"). IFN-λ1 mRNA was measured by RT-qPCR and normalized to 18S rRNA. For **A,** IFN-λ1 mRNA levels are plotted normalized to the lytic+casp-i sample. In **B,** the lytic+casp-i treated samples were sorted based on tdTomato expression and the fold enrichment in IFN-λ1 RNA levels compared to unsorted ("bulk") samples is plotted in $\log_{10}$ scale. n=6.

Figure 3. TBK1 and IRF3 are activated even in cells that do not transcribe IFN-β. BC3-IFN-βp-tdTomato reporter cells were treated with 20 ng/ml TPA for 48 hours to induce the lytic cycle ("lytic (TPA)"). Where indicated, the cells were also treated with the pan-caspase inhibitor IDN-6556 at 10 μM ("casp-i"). Protein was isolated from treated cells without sorting ("bulk"), or, for the lytic+casp-i treated sample, after sorting based on tdTomato expression. Protein lysates were probed for phosphorylated IRF3 (Ser386), total IRF3, phosphorylated TBK1

(Ser172), total TBK1, and β-actin as a loading control. As a positive control for IRF3 and TBK1 activation/phosphorylation, A549 cells were treated with poly(I:C) for 6 and 48 hours before protein lysates were collected. Images shown are representative of 3 replicates.

Figure 4. Levels of the AP-1 subunit ATF2 and phosphorylation of the NF-κB subunit RelA are higher in IFN-β high cells. A-B. Re-analysis of single-cell RNA sequencing (scRNA-seq) data in Tabtieng, Lent et al 2022 (6). iSLK.219 cells were treated with 1 μg/mL doxycycline for 4 days to induce the lytic cycle ("lytic"). The cells were also treated with the pan-caspase inhibitor IDN-6556 at 10 μM ("casp-i"), as well as a mixture of antibodies against type I interferon and its receptor ("anti-IFN Abs") (**B** only) to block IFN-β paracrine signaling where indicated. Average mRNA levels of genes in the IFN-β enhanceosome from the scRNA-seq data are shown for each of the 12 clusters of cells identified by the original analysis. The IFN-β-positive clusters 9 and 11 were further separated into two groups based on the IFN-β status of individual cells. **C-G.** BC3-IFN-βp-tdTomato reporter cells were treated with 20 ng/ml TPA for 48 hours to induce the lytic cycle ("lytic (TPA)"). Where indicated, the cells were also treated with the pan-caspase inhibitor IDN-6556 at 10 μM ("casp-i") and with a mixture of antibodies against type I interferon and its receptor ("anti-IFN Abs") to block IFN-β paracrine signaling. The lytic+casp-i+anti-IFN Abs treated samples were also sorted based on tdTomato expression in D-G. **C-D.** IFN-β RNA was measured by RT-qPCR and normalized to 18S rRNA. In C, IFN-β RNA levels are plotted normalized to the lytic+casp-i sample. In D, the fold enrichment in IFN-β RNA levels is compared to unsorted ("bulk") samples plotted in $\log_{10}$ scale. n=4. **E-G.** Western blots of protein samples from unsorted ("bulk") and sorted cells. Protein lysates were probed for: (**E**) phosphorylated IRF3 (Ser386), total IRF3, (**F**) ATF2, c-Jun, (**G**) phosphorylated RelA (Ser536), total RelA, β-actin was used as loading control. Images shown are representative of 3 replicates.

Figure 5. Model of regulation of heterogeneous IFN-β expression by components of the IFN-β enhanceosome. *(Left)* In the rare cells that induce IFN-β during viral infection, there are high levels of the AP-1 factor ATF2 and the NF-κB subunit RelA becomes phosphorylated in addition to IRF3 in response to infection. This results in the formation of the IFN-β enhanceosome and IFN-β transcription. *(Right)* In the majority of virally infected cells, there are

lower amounts of ATF2, and RelA is not phosphorylated during infection. While IRF3 is still activated, the full IFN-β enhanceosome does not form and IFN-β is not induced.

Supplemental Figure 1. Controls showing efficient reactivation of BC3-IFN-βp-tdTomato and efficient block of interferon stimulate gene induction by anti-IFN antibodies. BC3-IFN-βp-tdTomato reporter cells were treated with 20 ng/ml TPA for 48 hours to induce the lytic cycle ("lytic"). Where indicated, the cells were also treated with the pan-caspase inhibitor IDN-6556 at 10 μM ("casp-i") and in **B and C** a mixture of antibodies against type I interferon and its receptor ("anti-IFN Abs") to block IFN-β paracrine signaling. The percentage of cells expressing the lytic KSHV protein ORF45 was measured by flow cytometry. Graphs A and B show the reactivation rates for all BC3 experiments shown (**A)** n=7, (**B**) n=5. **C.** mRNA levels of MxA, an interferon stimulated gene (ISG) were measured by qRT-PCR and normalized to 18S rRNA. n=4.

Supplemental Figure 2. Representative gating strategy for FACS. Plots showing an example gating for BC3-IFN-βp-tdTomato cell sorting based on tdTomato fluorescence. Gates for tdTomato-positive and negative populations were drawn conservatively to prevent false positives and negatives. In this particular experiment, BC3-IFN-βp-tdTomato reporter cells were treated with 20 ng/ml TPA and 10 μM IDN-6556 (IDN) for 48 hours to induce the lytic cycle and trigger IFN-β expression and tdTomato production. Side scatter (SSC) and forward scatter (FSC) area (A) and height (H) were used to separate cells from debris and remove doublets. DAPI staining was used to identify live cells. Cells thus gated were sorted based on tdTomato expression in comparison to BC-3 cells lacking the reporter. tdTomato was plotted against green fluorescence, as autofluorescence is detected in the green channel. Gates indicated by red and cyan colors were set for collecting tdTomato-positive and negative cells, respectively.

Supplemental Figure 3. Lack of IFN signaling induction by TPA and caspase inhibitors in uninfected B cells. BJAB cells were treated with 20 ng/ml TPA and/or the pan-caspase inhibitor IDN-6556 at 10 μM ("casp-i") for 48 hrs. BC-3 cells treated with TPA and IDN-6556 were used as a positive control for induction of type I and III interferons. IFN-β (**A**) and IFN-λ1 (**B**) mRNA levels were measured by qRT-PCR and normalized to 18S rRNA. Their levels are plotted

normalized to TPA and IDN-6556-treated BC-3 sample. n=4. **C.** Protein lysates were probed with antibodies against phosphorylated IRF3 (Ser386), total IRF3, phosphorylated TBK1 (Ser172), total TBK1, ATF2, c-Jun, total RelA, phosphorylated RelA (Ser536), and β-actin as loading control. Images shown are representative of 3 replicates.

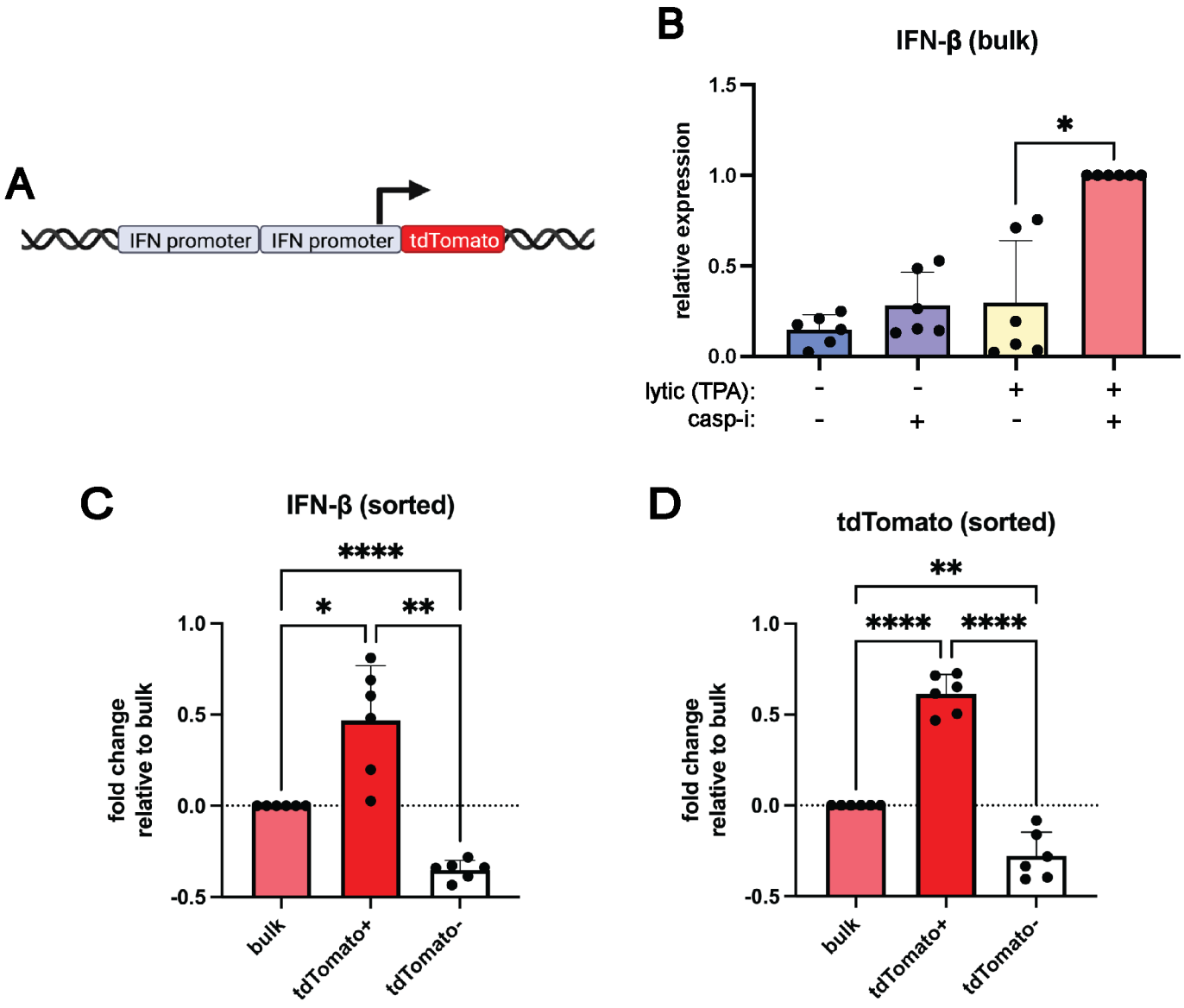

Figure 1. An IFN-β-promoter driven fluorescent reporter allows isolation of cells expressing high and low levels of IFN-β. A. Diagram of the IFN-βp-tdTomato reporter. Two copies of the 303 bp minimal promoter sequence for the human IFNB1 gene were cloned in front of the tdTomato fluorophore. This cassette was then introduced in BC-3 cells via lentiviral transduction leading to stable integration. **B-D.** BC3-IFN-βp-tdTomato reporter cells were treated with 20 ng/mL TPA for 48 hours to induce the lytic cycle ("lytic (TPA)") . Where indicated, the cells were also treated with the pan-caspase inhibitor IDN-6556 at 10 μM ("casp-i"). IFN-β and tdTomato mRNA levels were measured by RT-qPCR and normalized to 18S rRNA. For **B**, IFN-β mRNA levels are plotted normalized to the lytic+casp-i sample . For **C and D** the lytic+casp-i treated samples were sorted based on tdTomato expression and the fold enrichment in IFN-β and tdTomato RNA levels compared to unsorted ("bulk") samples is plotted in log10 scale. n=6.

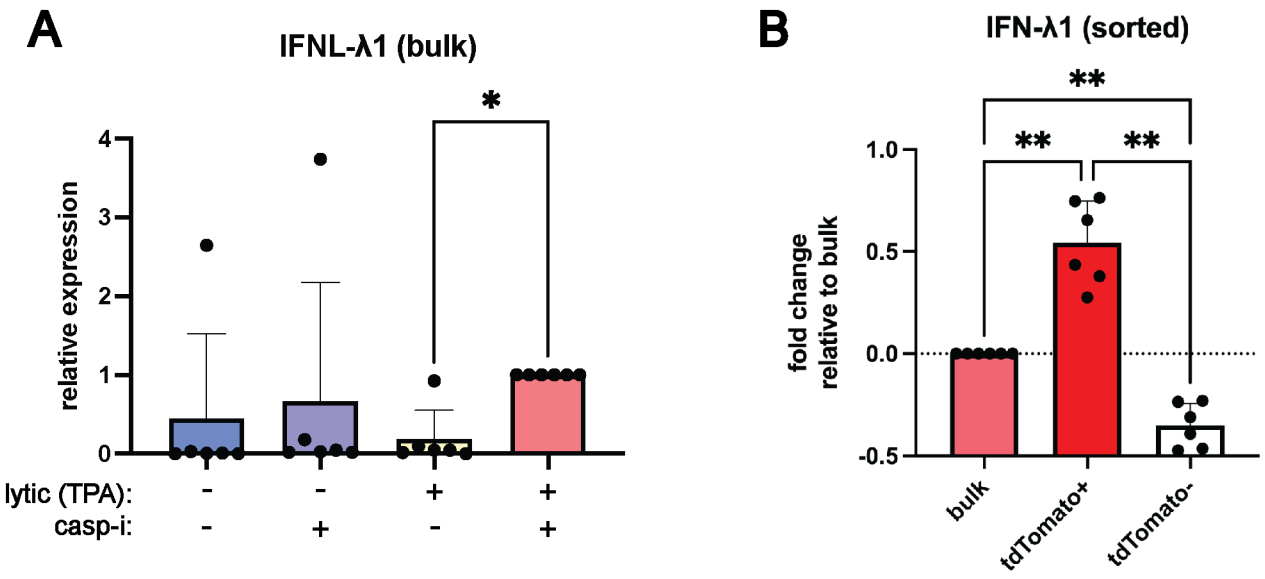

Figure 2. IFN-λ1 is expressed in the same set of cells that produce high levels of IFN-β, pointing to heterogeneity in the induction pathway rather than -stochastic IFN-β promoter firing. A. BC3-IFN-βp-tdTomato reporter cells were treated with 20 ng/ml TPA for 48 hours to induce the lytic cycle ("lytic (TPA)"). Where indicated, the cells were also treated with the pan-caspase inhibitor IDN-6556 at 10 μM ("casp-i"). IFN-λ1 mRNA was measured by RT-qPCR and normalized to 18S rRNA. For **A**, IFN-λ1 mRNA levels are plotted normalized to the lytic+casp-i sample. In **B**, the lytic+casp-i treated samples were sorted based on tdTomato expression and the fold enrichment in IFN-λ1 RNA levels compared to unsorted ("bulk") samples is plotted in log10 scale. n=6.

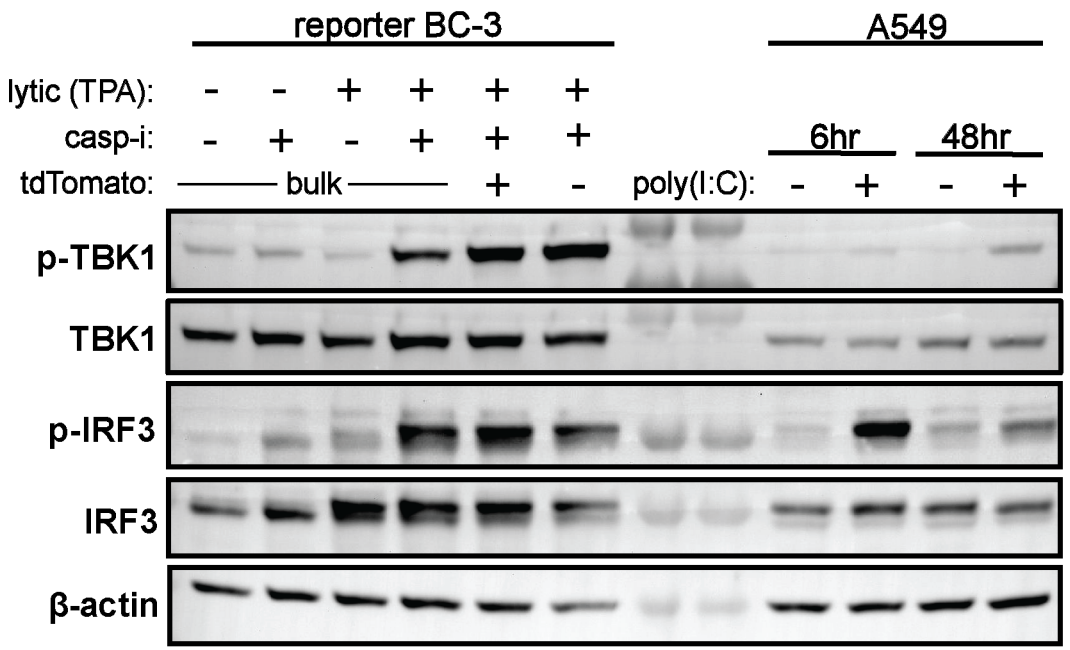

Figure 3. TBK1 and IRF3 are activated even in cells that do not transcribe IFN-β. BC3-IFN-βp-tdTomato reporter cells were treated with 20 ng/ml TPA for 48 hours to induce the lytic cycle ("lytic (TPA)"). Where indicated, the cells were also treated with the pan-caspase inhibitor IDN-6556 at 10 μM ("casp-i"). Protein was isolated from treated cells without sorting ("bulk"), or, for the lytic+casp-i treated sample, after sorting based on tdTomato expression. Protein lysates were probed for phosphorylated IRF3 (Ser386), total IRF3, phosphorylated TBK1 (Ser172), total TBK1, and β-actin as a loading control. As a positive control for IRF3 and TBK1 activation/ phosphorylation, A549 cells were treated with poly(I:C) for 6 and 48 hours before protein lysates were collected. Images shown are representative of 3 replicates.

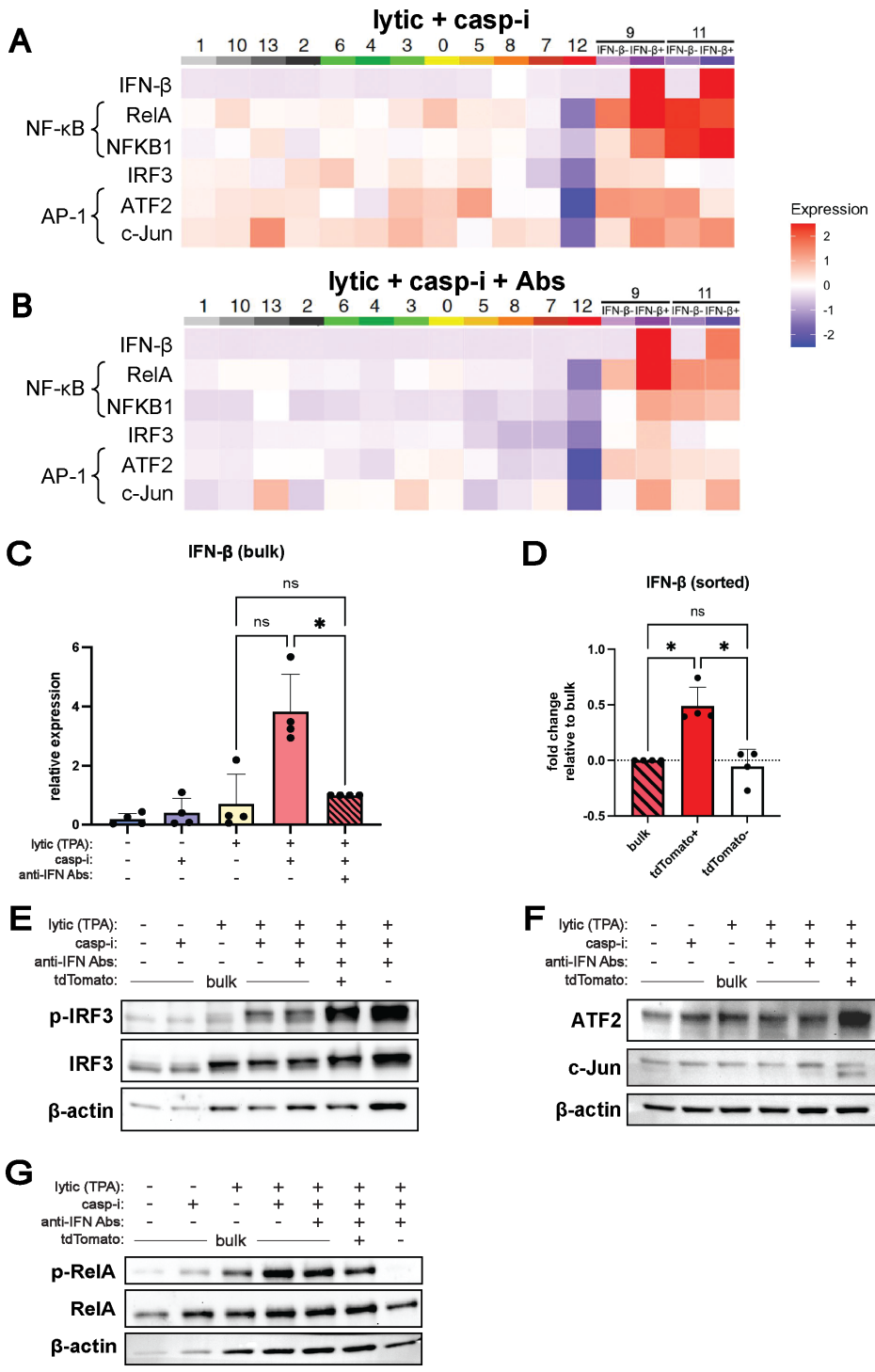

Figure 4. Levels of the AP-1 subunit ATF2 and phosphorylation of the NF-κB subunit RelA are higher in IFN-β high cells. A-B. Re-analysis of single cell RNA sequencing (scRNA-seq) data in Tabtieng, Lent et al 2022. iSLK.219 cells were treated with 1 µg/mL doxycycline for 4 days to induce the lytic cycle ("lytic"). The cells were also treated with the pan-caspase inhibitor IDN-6556 at 10 µM ("casp-i"), as well as a mixture of antibodies against type I interferon and its receptor ("anti-IFN Abs") (**B** only) to block IFN-β paracrine signaling where indicated. Average mRNA levels of genes in the IFN-β enhanceosome from the scRNA-seq data are shown for each of the 12 clusters of cells identified by the original analysis. The IFN-β-positive clusters 9 and 11 were further separated into two groups based on the IFN-β status of individual cells. **C-G.** BC3-IFN-βp-tdTomato reporter cells were treated with 20 ng/ml TPA for 48 hours to induce the lytic cycle ("lytic (TPA)"). Where indicated, the cells were also treated with the pan-caspase inhibitor IDN-6556 at 10 µM ("casp-i") and with a mixture of antibodies against type I interferon and its receptor ("anti-IFN Abs") to block IFN-β paracrine signaling. The lytic+casp-i+anti-IFN Abs treated samples were also sorted based on tdTomato expression in D-G. **C-D.** IFN-β RNA was measured by RT-qPCR and normalized to 18S rRNA. In C, IFN-β RNA levels are plotted normalized to the lytic+casp-i sample. In D, the fold enrichment in IFN-β RNA levels is compared to unsorted ("bulk") samples plotted in log10 scale. n=4. **E-G.** Western blots of protein samples from unsorted ("bulk") and sorted cells. Protein lysates were probed for: (**E**) phosphorylated IRF3 (Ser386), total IRF3, (**F**) ATF2, c-Jun, (**G**) phosphorylated RelA (Ser536), total RelA, β-actin was used as loading control. Images shown are representative of 3 replicates.

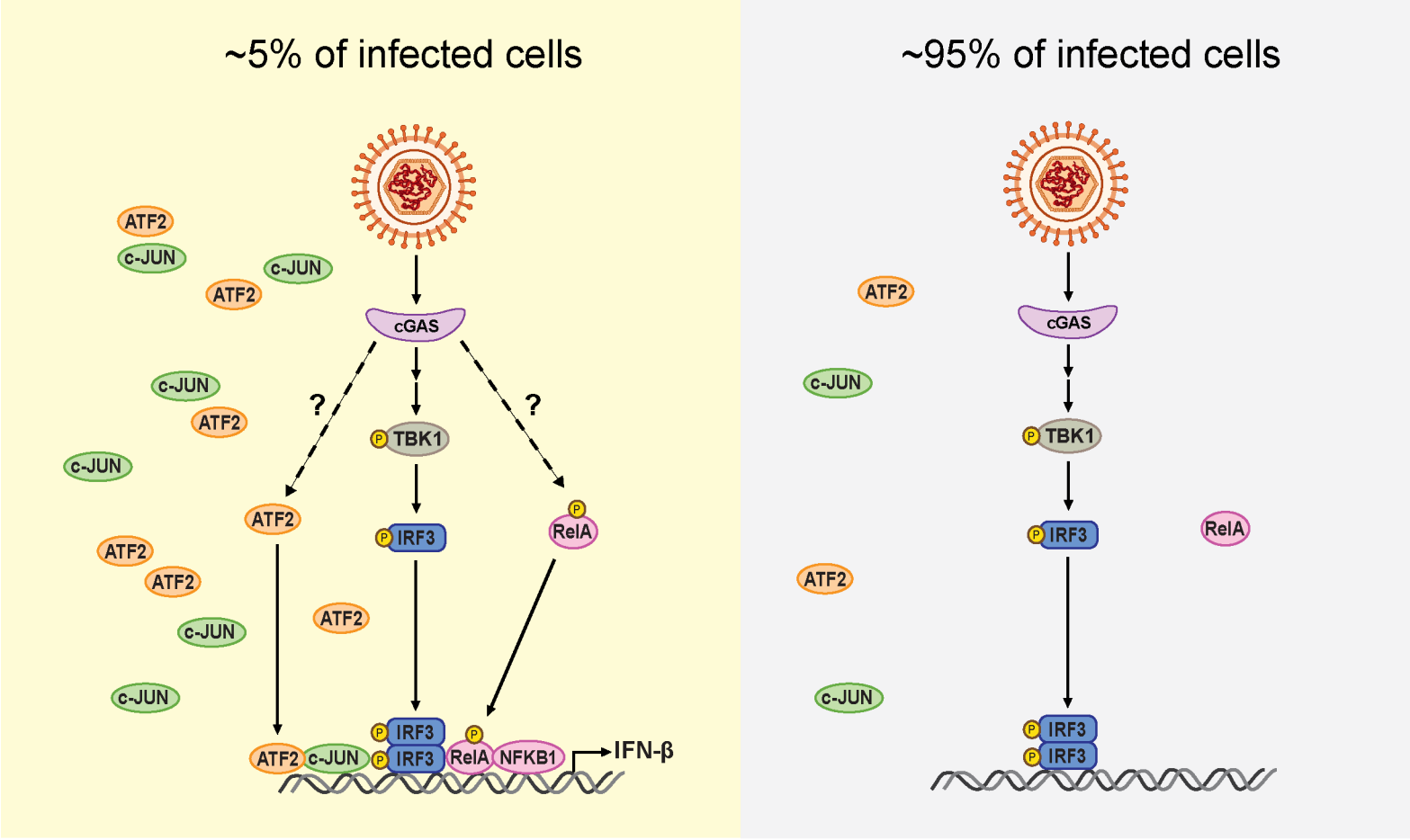

Figure 5. Model of regulation of heterogeneous IFN-β expression by components of the IFN-β enhanceosome. (Left) In the rare cells that induce IFN-β during viral infection, there are high levels of the AP-1 factor ATF2 and the NF-κB subunit RelA becomes phosphorylated in addition to IRF3 in response to infection. This results in the formation of the IFN-β enhanceosome and IFN-β transcription. (Right) In the majority of virally infected cells, there are lower amounts of ATF2, and RelA is not phosphorylated during infection. While IRF3 is still activated, the full IFN-β enhanceosome does not form and IFN-β is not induced.

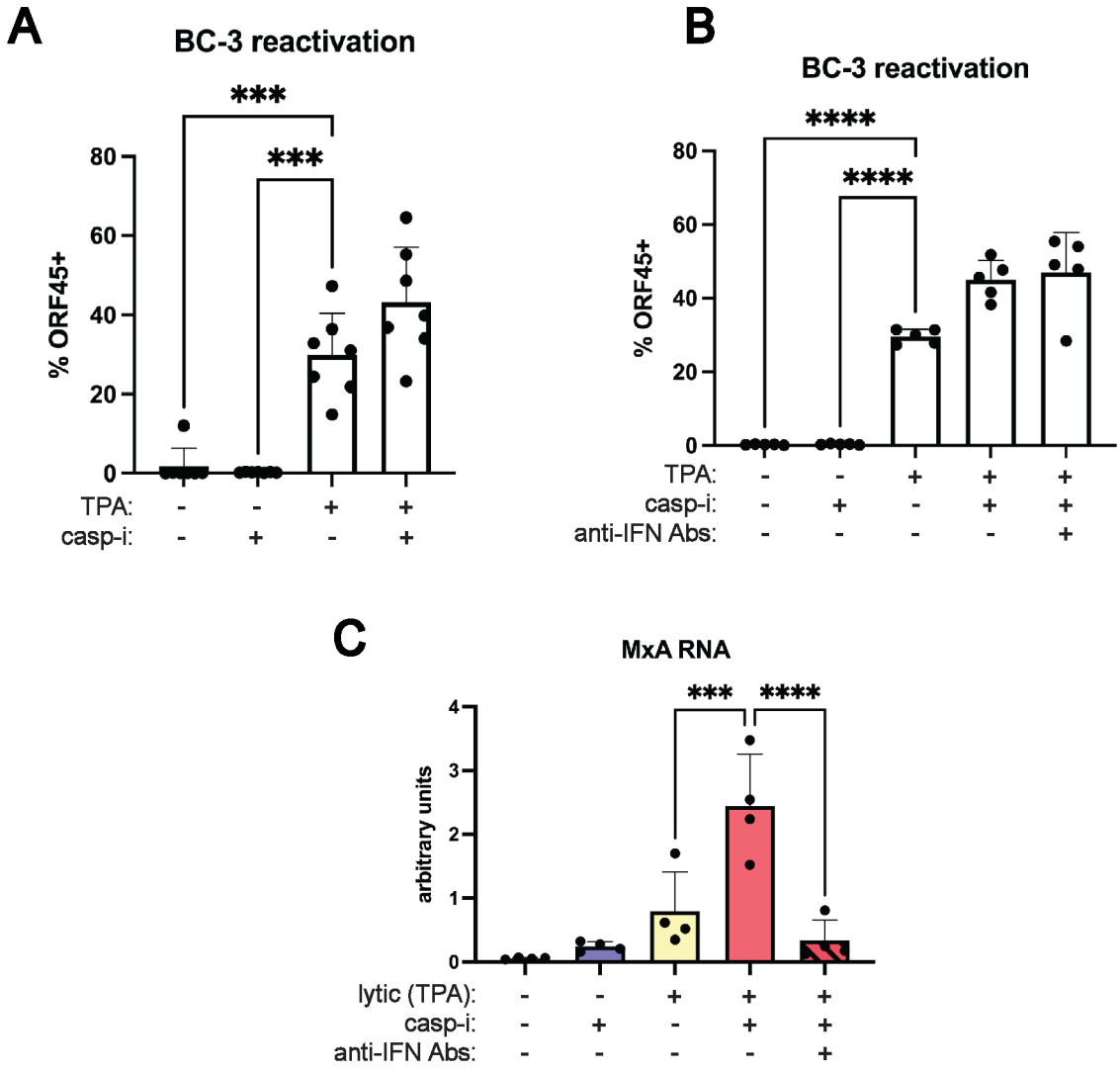

Supplemental Figure 1. Controls showing efficient reactivation of BC3-IFN-βp-tdTomato and efficient block of interferon stimulate gene induction by anti-IFN antibodies. BC3-IFN-βp-tdTomato reporter cells were treated with 20 ng/ml TPA for 48 hours to induce the lytic cycle ("lytic"). Where indicated, the cells were also treated with the pan-caspase inhibitor IDN-6556 at 10 μM ("casp-i") and in **B and C** a mixture of antibodies against type I interferon and its receptor ("anti-IFN Abs") to block IFN-β paracrine signaling. The percentage of cells expressing the lytic KSHV protein ORF45 was measured by flow cytometry. Graphs A and B show the reactivation rates for all BC3 experiments shown (**A**) n=7, (**B**) n=5. **C.** mRNA levels of MxA, an interferon stimulated gene (ISG) were measured by qRT-PCR and normalized to 18S rRNA. n=4.

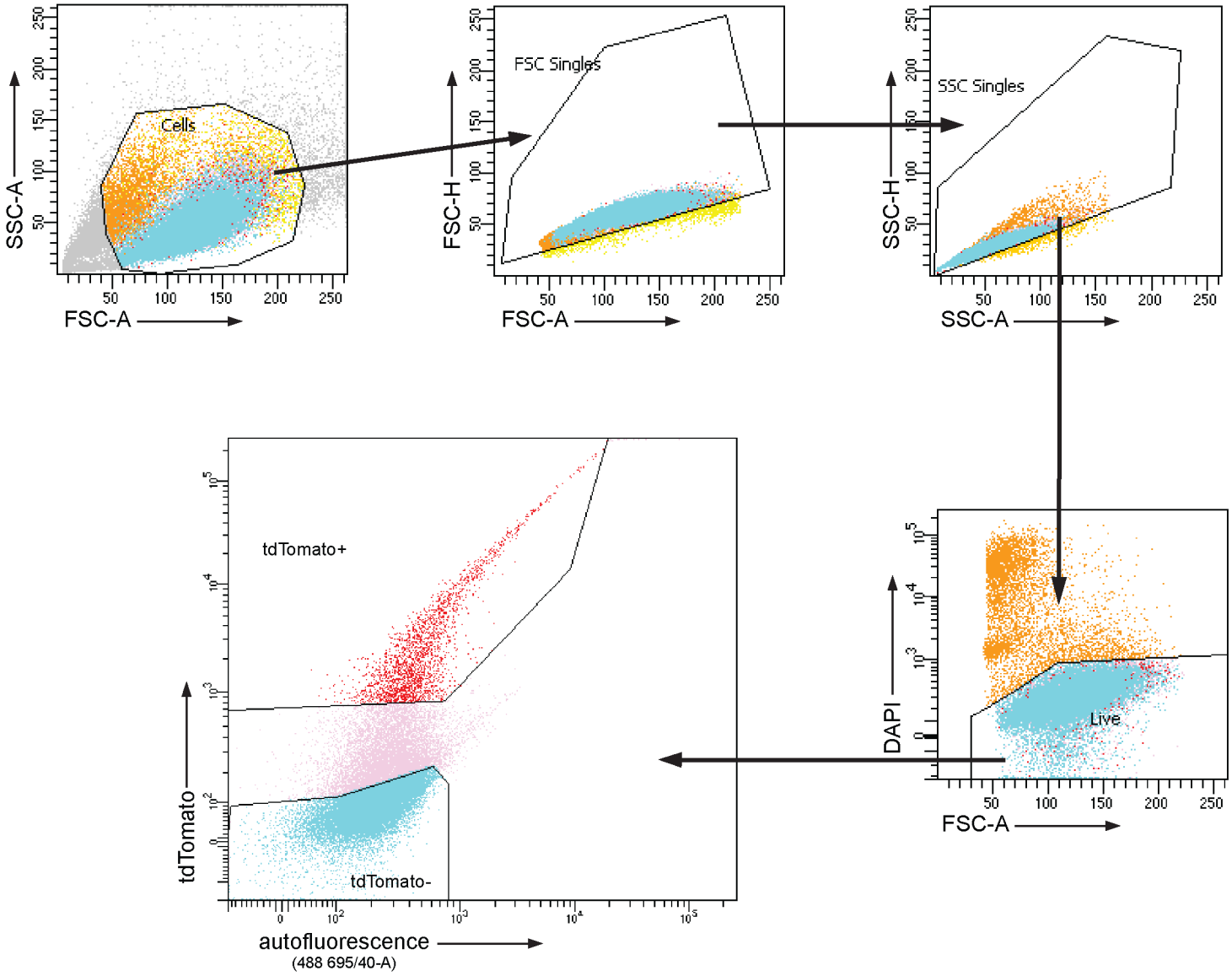

Supplemental Figure 2. Representative gating strategy for FACS. Plots showing an example gating for BC3-IFN-βp-tdTomato cell sorting based on tdTomato fluorescence. Gates for tdTomato-positive and negative populations were drawn conservatively to prevent false positives and negatives. In this particular experiment, BC3-IFN-βp-tdTomato reporter cells were treated with 20 ng/ml TPA and 10 μM IDN-6556 (IDN) for 48 hours to induce the lytic cycle and trigger IFN-β expression and tdTomato production. Side scatter (SSC) and forward scatter (FSC) area (A) and height (H) were used to separate cells from debris and remove doublets. DAPI staining was used to identify live cells. Cells thus gated were sorted based on tdTomato expression in comparison to BC-3 cells lacking the reporter. tdTomato was plotted against green fluorescence, as autofluorescence is detected in the green channel. Gates indicated by red and cyan colors were set for collecting tdTomato-positive and negative cells, respectively.

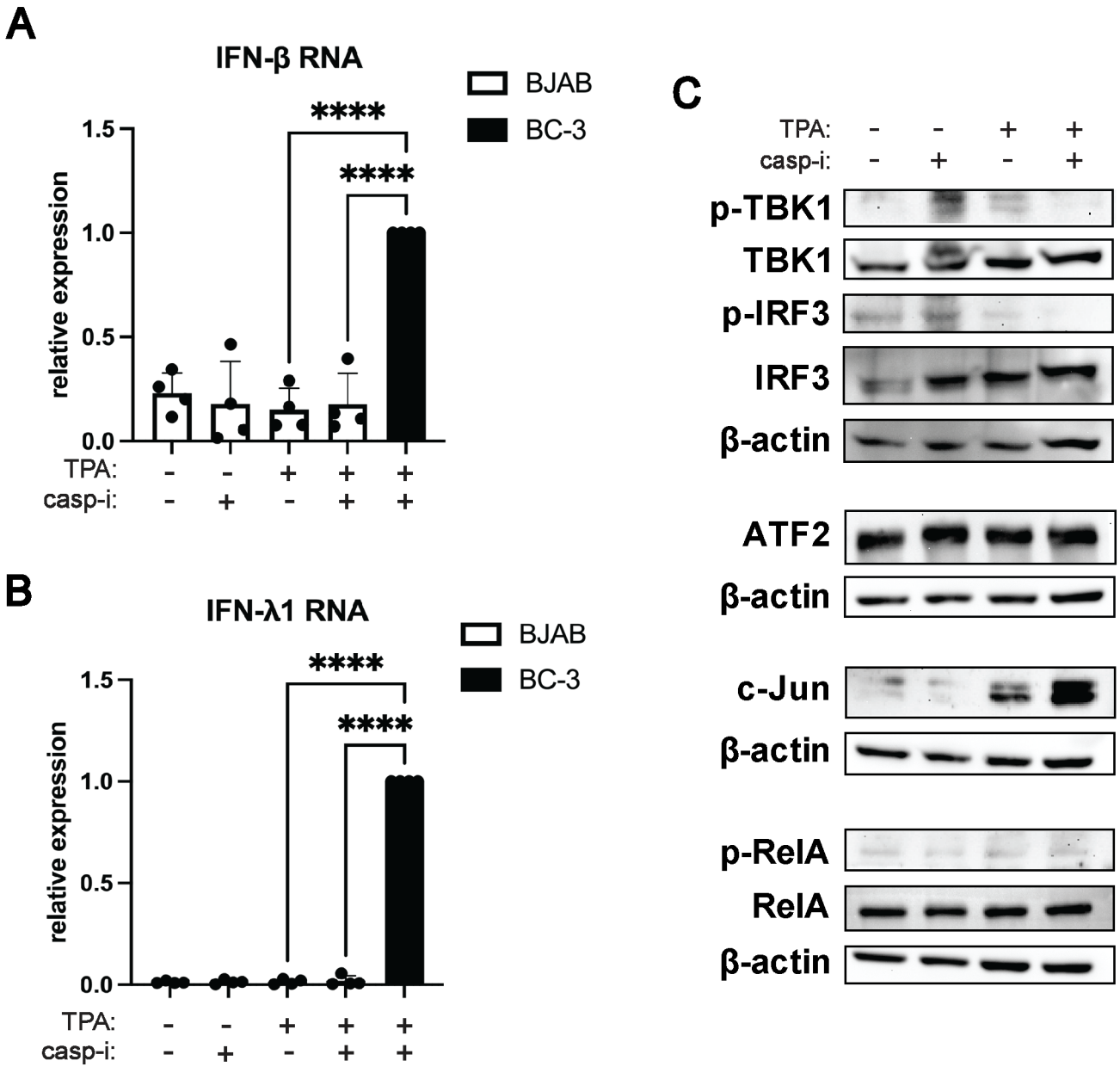

Supplemental Figure 3. Lack of IFN signaling induction by TPA and caspase inhibitors in uninfected B cells. BJAB cells were treated with 20 ng/ml TPA and/or the pan-caspase inhibitor IDN-6556 at 10 μM ("casp-i") for 48 hrs. BC-3 cells treated with TPA and IDN-6556 were used as a positive control for induction of type I and III interferons. IFN-β (**A**) and IFN-λ1 (**B**) mRNA levels were measured by qRT-PCR and normalized to 18S rRNA. Their levels are plotted normalized to TPA and IDN-6556-treated BC-3 sample. n=4. **C.** Protein lysates were probed with antibodies against phosphorylated IRF3 (Ser386), total IRF3, phosphorylated TBK1 (Ser172), total TBK1, ATF2, c-Jun, total RelA, phosphorylated RelA (Ser536), and β-actin as loading control. Images shown are representative of 3 replicates.